Cong *et al. Biochar* (2025) 7:97
https://doi.org/10.1007/s42773-025-00500-z

Biochar

ORIGINAL RESEARCH Open Access

Improved adsorption capacity of ammonium from aqueous solution by modified biogas residue biochar

Ping Cong[1†], Shuhui Song[2†], Yanmei Zhu[3†], Xinwei Ji[3], Shuai Liu[3], Shuai Kuang[1], Yanli Xu[1], Qiuqiang Hou[3], Xuebo Zheng[1*] and Wenjing Song[1*]

Abstract

Residue biochar can be utilized as an adsorbent for ammonium nitrogen (NH_4^+-N) to prevent non-point source pollution. However, the limited adsorption capacity has restricted its extensive application. In this study, biochar was modified with hydrogen peroxide (**H_2O_2**), potassium permanganate ($KMnO_4$), and sodium hydroxide (NaOH) to enhance its adsorption performance. A comparative analysis of the biochar surface characteristics was used to investigate the adsorption systems. The results indicated that the adsorption capacities of the modified biochar (MB) were significantly enhanced compared with the raw biochar (RB). At the highest NH_4^+-N concentration of 150 mg L^{-1}, the adsorption capacities of RB-H_2O_2, RB-NaOH, and RB-$KMnO_4$ increased to 3.0, 3.2, and 4.0 times that of RB, respectively. As predicted by the Langmuir isotherm model, the maximum adsorption capacities of these three MB were 13.93, 41.00, and 68.15 mg g^{-1}, respectively. Ammonium adsorption on the MB surfaces was affected by surface adsorption, liquid membrane diffusion, and intra-particle diffusion. The specific surface area and pore volume of RB-$KMnO_4$ were significantly enhanced, with an increase in active sites on the pore surfaces, thereby strengthening its adsorption capacity for NH_4^+-N. In contrast, the adsorption of NH_4^+-N by RB-H_2O_2 and RB-NaOH primarily relied on the substantial increase in –C–O functional groups, with additional contributions from other oxygen-containing functional (e.g. –OH, –COOH, and Fe–O). In conclusion, RB-$KMnO_4$ exhibited the highest adsorption efficiency, with pore-based adsorption playing a dominant role over functional group-based adsorption. These findings highlight the critical role of pore structure optimization in enhancing the biochar adsorption capacity for NH_4^+-N.

Highlights

- The biogas residue biochar was modified using H_2O_2, $KMnO_4$ and NaOH.
- RB-$KMnO_4$ created a superior ammonium adsorption capacity because of its exceptional pore structure.
- RB-H_2O_2 and RB-NaOH showed an enhanced adsorption performance attributed to its increased surface –C–O functional groups.
- Enhancing the pore structure of biochar more effectively boosted ammonium ion adsorption capacity.

[†]Ping Cong, Shuhui Song, and Yanmei Zhu have contributed equally to this work.

*Correspondence:
Xuebo Zheng
zhengxuebo@caas.cn
Wenjing Song
songwenjing@caas.cn
Full list of author information is available at the end of the article

Keywords Residue biochar modification, Ammonium nitrogen, Adsorption capacity, Pore-based adsorption, Functional group-based adsorption

Graphical Abstract

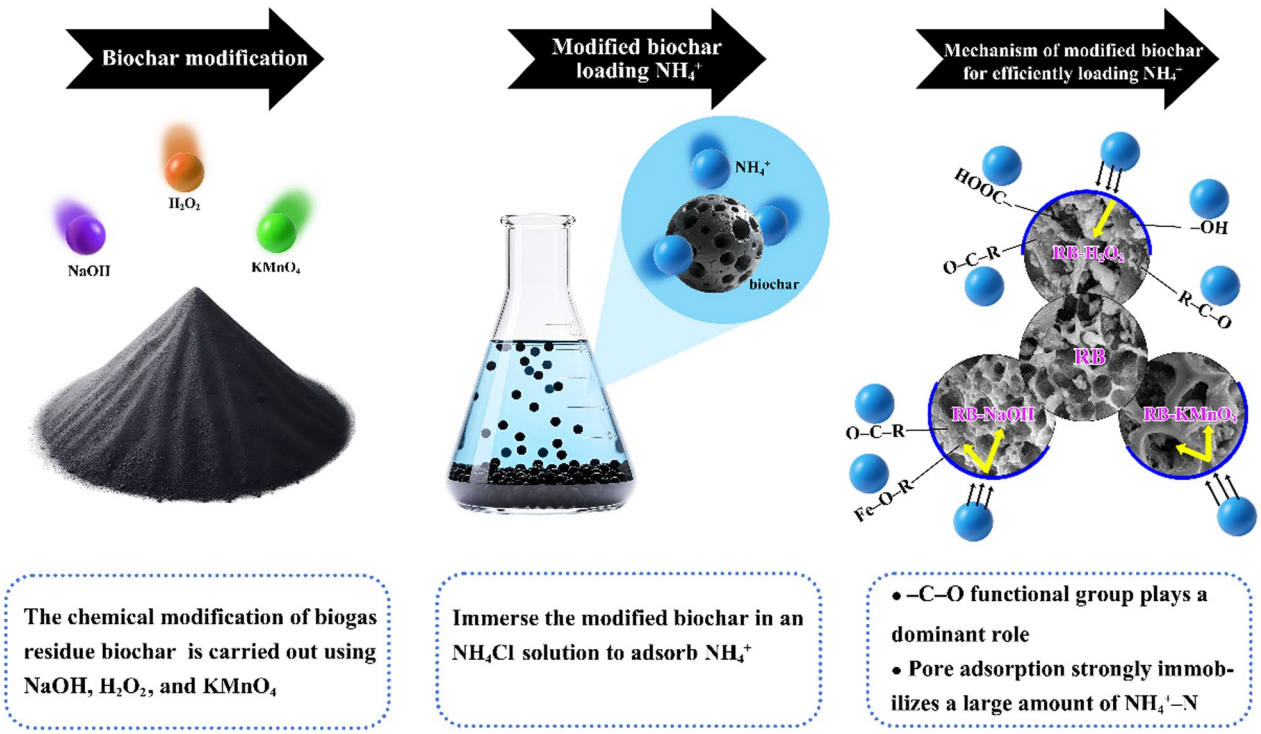

1 Introduction

Biochar, a carbon-rich, porous material, is derived from organic feedstock through a thermal combustion process involving limited oxygen at temperatures ranging from 200 to 700 ℃ (Gsior and Tic 2016). Various organic wastes such as agricultural and biogas residues can serve as feedstocks for biochar production. Biochar not only has exceptional porosity, large specific surface area (SSA), high cation-exchange capacity, and low electrical conductivity (EC), but also has robust adsorption capability, which can adsorb different forms of nitrogen and reduce nitrogen loss in farmland. This provides feasibility for solving the problem of non-point source pollution caused by excessive nitrogen in farmland (Li et al. 2018; Kaur et al. 2021).

Ammonia nitrogen (NH_4^+-N) is one of the main indicators of agricultural non-point source pollution, which mainly comes from fertilizer application, livestock and poultry breeding emissions, and farmland drainage in agricultural activities (Feng et al. 2023a, b; Li et al. 2023). It is necessary to take measures to adsorb NH_4^+-N, which can maintain soil acid–base balance, protect farmland water environment, ensure crop safety and human health (Raza et al. 2020; Zhu et al. 2024). Therefore, developing a novel efficient biochar material for adsorbing NH_4^+-N has become the focus of our work. However, previous studies showed that the adsorption capacity of raw biochar (RB) for NH_4^+-N was only 3–7 mg g^{-1} (Zheng et al. 2020; Hailegnaw et al. 2019). The adsorption limit of the 0–10 cm soil layer is 1.11 mg g^{-1}, which is much lower than our fertilization amount (Wang et al. 2022). Even with the application of biochar, only 9–20% of the NH_4^+-N can be adsorbed, and there is still a risk of NH_4^+-N migrating to groundwater (Liu et al. 2019; Wang et al. 2022). Therefore, it is urgent to take effective measures to increase the load amount of NH_4^+-N on biochar.

The reason why biochar, a carbon-based material, has good adsorption capacity is due to its inherent characteristics such as high porosity, large specific surface regions, and rich surface functional groups (Duygan et al. 2021; Rashid et al. 2021). The types of raw materials used in the preparation of biochar, the conditions for biochar

preparation, and the methods of biochar modification are all important factors that affect the expression of these characteristics (Tan et al. 2023; Wang et al. 2023). It was found that biochar prepared at 60 min and 5.0 °C min^{-1} under 700 °C presented the best development of smaller microporous and highest Brunauer–Emmett–Teller surface area of biochar in our previous studies (Cong et al. 2022; Zheng et al. 2020). However, the effectiveness of improving biochar characteristics by controlling preparation conditions is limited. Therefore, the focus has been shifted to the exploration of improving the loading capacity of NH_4^+-N through biochar modification. Previous studies have found that modified biochar (MB) can greatly improve its adsorption capacity, among which acid, alkali, and metal ion treatments are modification methods that can increase adsorption capacity (Shi et al. 2013; Qin 2017; Shang 2019; Sun 2020). Normally, a higher pH value is beneficial for the adsorption of NH_4^+-N, as NH_4^+ is more easily dissociated into ammonia (NH_3), which is more easily adsorbed (Jiang et al. 2024). In contrast, strong acid treatment may lead to the destruction of some active sites, while metal ion amendments, although able to introduce specific adsorption sites, may affect the porous structure of biochar itself, thereby reducing its overall adsorption capacity (Liu et al. 2024a). Therefore, in this case, more consideration is given to using strong bases as modifiers. The advantages of strong oxidants as modifiers are more reflected in their ability to significantly alter the surface chemical properties of biochar. Some strong oxidants can introduce more oxygen-containing functional groups on the surface of biochar, such as carboxyl (–COOH), hydroxyl (–OH), etc. These functional groups can increase the negative charge density of the biochar surface, thereby enhancing the electrostatic attraction to cations such as NH_4^+-N (Liu et al. 2024b). Numerous acidic functional groups (e.g., carboxyl groups, phenolic hydroxyl groups, hydrocarbon bonds, and hydroxyl and ethylenic bonds) have been reported to enhance the adsorption capacity of biochar derived from crop straw and oak sawdust (Wang et al. 2015; Liang et al. 2016). The improvement in acidic oxygen-containing functional groups and the formation of novel substituents, cationic exchange, and surface complexation of oxygen-containing functional groups, including carbohydrate C–OH and carboxylic C=O (C–O), significantly contributed to the adsorption of NH_4^+-N in the modified biochar (Cao and Harris 2010; Hou et al. 2016; Yu et al. 2016; Zhang et al. 2020; Chen et al. 2021). Through oxidation, more micropores and mesopores can be formed on the surface of biochar, increasing the specific surface area and providing more adsorption sites. In addition, strong alkali treatment can further optimize pore structure and improve adsorption performance by removing some ash and minerals (Chen et al. 2022).

Obviously, the adsorption of ammonium onto biochar is mainly influenced by its surface characteristics and pore structure. From the perspective of adsorbing NH_4^+-N, strong bases and strong oxidants have better applicability. However, it is not clear whether these modifiers can significantly increase the adsorption capacity of biochar for NH_4^+-N, and the adsorption mechanisms of different modifiers are also unclear. In this study, biogas residue (BR) was still used as the raw material for preparing biochar based on previous experimental results. The carbonization utilization of biogas residue waste is of great significance for the development of biogas engineering, ecological environment construction, and the development of green and low-carbon agriculture (Chen et al. 2021; Ragauskas et al. 2006; Stefaniuk et al. 2016). Hydrogen peroxide (H_2O_2), potassium permanganate ($KMnO_4$), and sodium hydroxide (NaOH) were selected as modifiers to modify biochar from BR. We assume that these modifiers alter the pore structure and surface functional groups of the original biochar, resulting in a significant increase in the adsorption performance of biochar, manifested in a sharp improvement in the adsorption quantity of NH_4^+-N. Thus, this study aims to (i) prepare and characterize modified biochar for NH_4^+-N adsorption, (ii) investigate the kinetics and isotherms of NH_4^+-N adsorption by RB-H_2O_2, RB-$KMnO_4$, and RB-NaOH, and (iii) elucidate the mechanisms underlying NH_4^+-N adsorption by MB.

2 Materials and methods

2.1 Materials

The precursor substance employed in the biochar synthesis was obtained from an Anaerobic Digestion Residue (ADR), a byproduct of the aerobic digestion process of distillery grains (DG). This process took place in a 500 m^3 biogas plant situated in Pingdu town, Qingdao, China (36° 28′ N, 119° 35′ E). Comprehensive information concerning the production and characteristics of the ADR-DG has been thoroughly discussed in previous studies (Zheng et al. 2018a, b). The processing method and characteristics of BR before preparing it into biochar are detailed in the supplementary materials.

The residue biochar was prepared based on parameters such as the maximum adsorption capacity for NH_4^+, the optimal residence time (RT) during pyrolysis, and the heating rate (HR), as reported in our previous study (Zheng et al. 2021). The detailed preparation procedure is provided in the Supplementary Materials. The prepared RB was used for subsequent modification experiments, and its fundamental physicochemical properties are presented in Table 1.

Table 1 The basic characteristic of unmodified and modified biochars

	RB	RB-H_2O_2	RB-$KMnO_4$	RB-NaOH
C%	59.61 ± 1.24c	60.78 ± 0.45b	79.51 ± 0.62a	58.93 ± 0.61c
H%	2.54 ± 0.39a	1.65 ± 0.02b	2.65 ± 0.29a	2.8 ± 0.08a
N%	1.24 ± 0.03c	1.42 ± 0.03b	1.89 ± 0.03a	1.25 ± 0.02c
S%	1.83 ± 0.15a	0.55 ± 0.02d	0.92 ± 0.14c	1.15 ± 0.06b
C/N	50.28	43.98	43.21	49.29
C/H	27.38	32.87	29.85	22.12
pH	10.95 ± 0.01a	9.79 ± 0.02c	10.60 ± 0.01b	8.46 ± 0.03d
ash%	0.48 ± 0.02a	0.47 ± 0.05a	0.53 ± 0.02a	0.15 ± 0.06b
pH_{pzc}	6.97	6.98	8.26	6.46

2.2 Biochar modification

2.2.1 Hydrogen peroxide modification

The 2-h dispersion of 3 g of biochar in 20 mL of 15% H_2O_2 solution was conducted at room temperature, followed by three rinses with deionized water. After each rinse, the biochar was filtered using a 0.45 μm membrane, and was dried at 80 ℃.

2.2.2 NaOH modification

A 10 g sample of biochar was accurately weighed and placed in a Teflon beaker. Subsequently, 20 mL of 5 mol L^{-1} NaOH solution was added (Teli et al. 2024). The mixture was heated at 70 ℃ for a duration of 4 h. The first drying of material was made in a Muffle furnace at 110 ℃, followed by 2-h heating at 600 °C under N_2 gas (10 psi = 68.95 kPa). The biochar was subjected to multiple rounds of rinsing with distilled water, resulting in the production of modified biochars. The modification process was considered complete when the pH of the rinse solution was approximately 7. After each rinse, the biochar was filtered with a 0.45 nm filter membrane, and dried at 70 ℃.

2.2.3 $KMnO_4$ modification

20 g of biochar was dispersed into 100 mL of 0.1 mol L^{-1} $KMnO_4$ solution over 2 h. The solution was sonicated, and then dried for 24 h at 80 ℃. The material was placed in a Muffle furnace continuously filled with nitrogen to ensure an anaerobic environment. The temperature of the muffle furnace was adjusted to 600 ℃ for pyrolysis for 1 h. The resulting modified material was thoroughly rinsed three times with deionized water. After each rinse, the material was filtered through a 0.45 nm filter membrane and then dried at 80 ℃.

2.3 Characterization of biochar

A Hitachi (SU-70, Japan) microscope was used to capture scanning electron microscope (SEM) images (5000 × magnification). The specific surface areas (SSA) and pore structures of the samples were evaluated using the Brunauer–Emmett–Teller (BET) method. Nitrogen (N_2) adsorption measurements were performed at 77 K using an ASAP 2020 M + C instrument (Micromeritics, USA). Each sample, weighing between 0.07 and 0.08 g, was initially subjected to vacuum degassing with a heating rate of 10 ℃ min^{-1} up to 200 ℃, for a duration of 4 h prior to the measurements. The Barrett-Joyner-Halenda (BJH) approach was then used for the adsorption data to determine the pore diameter, overall pore volume (Vt), ore volume (Vmic), and mesopore volume (Vmes).

Additionally, the surface functional groups were characterized using Fourier-transform infrared spectroscopy (FTIR). The FTIR analysis was performed on a Nicolet 6700 (Thermo Scientific, USA) within the wavenumber range of 400–4000 cm^{-1} using the KBr pellet technique. About 1.0 wt% of each sample was mixed with KBr to obtain discernible spectra. The omnic spectral analysis with OriginPro2021 (OriginLab, USA) was used to describe the significant spectral features.

The thermogravimetric (TG) and derivative thermogravimetric (DTG) experiments were performed to assess the thermal characteristics of the BR sample. These explorations were conducted non-isothermally using a TAG analyzer (Rubotherm Dyntherm HP, Netherlands) within temperature range of 25–800 ℃. Approximately 50 mg of the BR sample was utilized for the analysis under a nitrogen flow of 50 cm min^{-1} and a heating rate of 5 ℃ min^{-1}. The TG and DTG curves were then plotted as functions of temperature. Furthermore, quantitative analysis of organic elements including carbon (C), hydrogen (H), oxygen (O), and nitrogen (N) was performed with an element analyzer (EA, Elementar Vario EL III, Germany).

2.4 Ammonium nitrogen adsorption

The batch adsorption tests were performed following a specific procedure. Specifically, 3.819 g of ammonium chloride (NH_4Cl, certified A.C. S, Fisher Scientific) was dissolved in 1000 mL of deionized water to prepare a NH_4^+ stock solution of 1000 mg N L^{-1}. The NH_4^+ stock solution was diluted into 5, 10, 20, 50, 100 and 150 mg L^{-1} respectively with deionized water. Then, 40 mL of the above solution was transferred into a 50 mL centrifuge tube, and its pH was adjusted to 7.0. Then, 0.4 g of RB,

RB-H_2O_2, RB-$KMnO_4$, RB-NaOH had been added into the centrifuge tube to initiate the adsorption process. The mixed solution was shaken at 25 ℃ (140 rpm) for 120 h, centrifuged at 4000 rpm for 10 min, and passed through a 0.45 μm filter membrane.

The concentration of NH_4^+ in the filtrate was determined by Nessler's reagent spectrophotometry using an UV–VIS spectrophotometer (Evolution 220, Thermo Scientific, US) with an incident wavelength of 420 nm. The adsorptive capacity for NH_4^+-N was computed utilizing Eq. (1):

$$Q_e = (C_1C_2) \times V/m \tag{1}$$

where Q_e is the adsorption capacity (mg g^{-1}), C_1 is the initial concentration of NH_4^+-N (mg L^{-1}), C_2 is the consistency of NH_4^+-N after adsorption (mg L^{-1}), V is the volume of the solution (L), and m is the mass of the adsorbent material (g).

2.4.1 Adsorption kinetic research

Adsorption samples were collected at 3, 30, 60, 90, 120, 240, 480, 960, and 1440 min. The adsorption kinetics were evaluated using the pseudo-second- and first-orders, and intra-particle diffusion models, as shown in Eqs. (2), (3), (4), and (5).

Pseudo-first-order, nonlinear equation:

$$Q_t = Q_e \times \left(1 - e^{-k_1 t}\right) \tag{2}$$

where Q_t is the adsorption quantity at a certain time (mg g^{-1}), Q_e is the equilibrium adsorption capacity (mg g^{-1}), t is the adsorption time (min), and k_1 is the pseudo-first-order adsorption rate constant (min^{-1}).

Pseudo-second-order, nonlinear equation:

$$Q_t = \frac{Q_e^2 k_2 t}{1 + Q_e k_2 t} \tag{3}$$

where k_2 (g m g^{-1} min^{-1}) represents the pseudo-second-order rate constant.

Elovich:

$$Q_t = \frac{1}{\beta} ln(1 + \alpha\beta t) \tag{4}$$

where α is the primary rate constant (mg g^{-1} min^{-1}) and β is the desorption constant (mg g^{-1}).

Intra-particle diffusion:

$$Q_t = k_p t^{1/2} + C \tag{5}$$

where k_p is the rate constant relevant to the intra-particle diffusion model (mg g^{-1} $min^{-1/2}$). The constant C is associated with the thickness of the boundary layer (mg g^{-1}); a higher value of C implies a more pronounced influence on the limiting boundary layer.

2.4.2 Adsorption isotherm research

The adsorption isotherms were subsequently analyzed using the Langmuir, Freundlich, Temkin, and Dubinin-Radushkevich models, as shown in Eqs. (6), (7), (8), (9), (10), and (11).

Langmuir:

$$Q_e = \frac{Q_m K_L C_e}{1 + K_L C_e} \tag{6}$$

where K_L is the Langmuir adsorption isotherm constant (L mg^{-1}), Q_m is the maximum monolayer adsorption capacity (mg g^{-1}), Q_e (mg g^{-1}) is the equilibrium adsorption capacity, and C_e is the equilibrium ammonium concentration (mg L^{-1}).

Freundlichadsoption isotherm:

$$Q_e = K_F C_e^{1/n} \tag{7}$$

where K_F is the Freundlich adsorption capacity ($mg^{(1-1/n)}$ $L^{-1/n}$ g^{-1}). The Freundlich equation constant, 1/n (dimensionless), also referred to as the Freundlich adsorption intensity, signifies the reaction intensity between the ammonium molecules and adsorbent, which varies with the nonuniformity of the adsorbent. The value of 1/n is within the range of 0–1. A value within the range of 0.1 to 0.5 implies a higher adsorption intensity, suggesting favorable adsorption conditions.

In the context of the Temkin model, indirect mutual effects among adsorbates lead to a linear decline in the enthalpy of adsorption as a function of surface coverage. Consequently, the enthalpy of adsorption decreased linearly with the quantity of adsorbed species.

$$Q_e = \frac{RT}{b} ln(K_T C_e) \tag{8}$$

In this equation, b means a constant associated with the enthalpy of adsorption (J mol^{-1}), $b < 4.2$ kJ mol^{-1}. The equilibrium constant, K_T (L mg^{-1}), signifies the maximum binding energy in the context of material analysis and detection.

Dubinin-Radushkevich isotherm, adsorption by uniformed pores:

$$Q_e = Q_m e^{-K_{DR}\varepsilon^2} \tag{9}$$

$$\varepsilon = RTln\left(1 + \frac{1}{C_e}\right) \tag{10}$$

$$E = \frac{1}{\sqrt{2K_{DR}}} \tag{11}$$

where Q_m is the maximum adsorption capacity of ions (mg g^{-1}); K_{DR} is the Dubinin-Radushkevich (D-R) constant (mol^2 kJ^{-2}) related to the energy of adsorption. The Polanyi potential is symbolized by ε. The average free energy of adsorption is estimated by E (kJ mol^{-1}). It is noteworthy that when $1 < E < 16$ kJ mol^{-1}, physical adsorption is the leading function, whereas when $E > 16$ kJ mol^{-1}, chemisorption predominates. The universal gas constant is represented by R, with a value of 8.314 kJ mol^{-1}. T refers to the standard temperature, set at 298.15 K.

Furthermore, the factors influencing ammonium-nitrogen adsorption, including solution pH, competitive ions, and initial NH_4^+-N concentration, were also characterized and are detailed in the Supplementary Materials.

2.5 Statistical analysis

The collected data were subjected to one-way analysis of variance (ANOVA), followed by a post-hoc Duncan's multiple range test using SPSS Statistics software, version 25. The threshold for statistical significance was $P < 0.05$. All graphical representations were created using OriginPro2021 (OriginLab, USA).

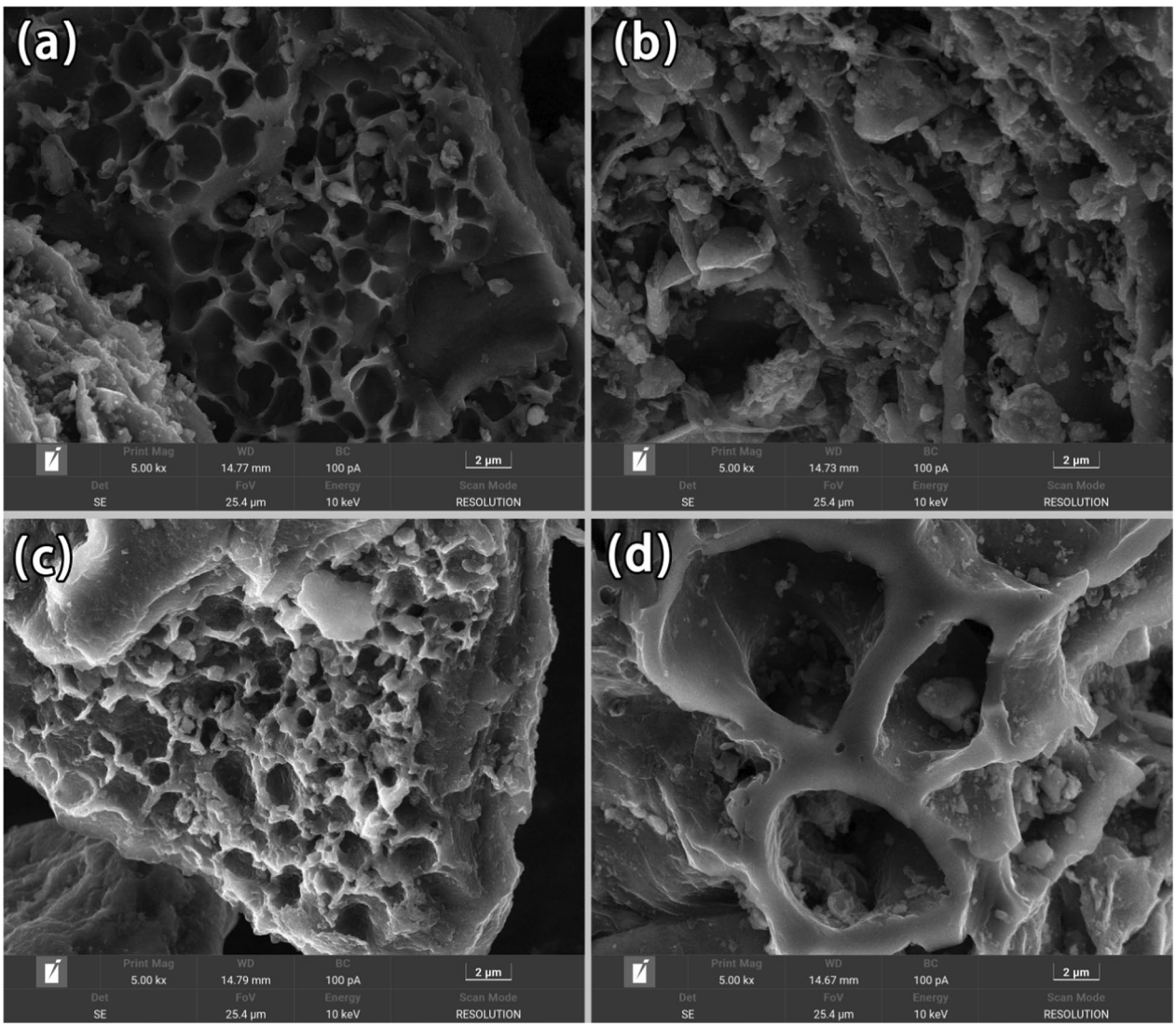

Fig. 1 The SEM images of biochars: RB (**a**), RB-H_2O_2 (**b**), RB-NaOH (**c**), RB-$KMnO_4$ (**d**). RB means residue biochar; RB-H_2O_2 means residue biochar modified by H_2O_2; RB-NaOH means residue biochar modified by NaOH; RB-$KMnO_4$ means residue biochar modified by $KMnO_4$

3 Results and discussion

3.1 Characterization of biochar

3.1.1 SEM

Figure 1 shows the SEM images of the morphological texture on the surface of RB and modified biochar (RB-H_2O_2, RB-NaOH, and RB-$KMnO_4$). Modifications with H_2O_2, NaOH, and $KMnO_4$ significantly altered the surface characteristics of the RB. The RB exhibited a honeycomb-like porous structure, with most of the pores being regularly shaped (Fig. 1a). After modification, the biochar morphology became notably rougher with porous structures displaying diverse shapes and sizes. In the RB-H_2O_2 sample, the rectangular pores were interconnected by adjacent pores (Fig. 1b), which could be attributed to the volatilization and release of organic compounds (Pariyar et al. 2020). Successful biochar loading was observed in the form of attachments on the surfaces of RB-NaOH and RB-$KMnO_4$ (Zhang et al. 2020). In particular, the pores of RB-$KMnO_4$ became more abundant and deeper, and the surface exhibited a significant collapse, thereby enhancing the roughness of the biochar surface (Fig. 1d).

3.1.2 Physicochemical properties of biochar

The pH in the MB treatment decreased significantly (Table 1). This implied an increase in the electronegative surface charge of the biochar (Qiu et al. 2008; Tripathy et al. 2021). The enhancement in electronegativity was demonstrated to be beneficial for the adsorption of NH_4^+-N. Upon modification, the sulfur content of the biochar notably diminished, whereas the carbon and nitrogen contents of the RB-$KMnO_4$ increased. The C/H ratio and ash content of RB-NaOH decreased, indicating weakening of the aromatic construction of the biochar and an improvement in its hydrophilicity, which facilitated the fixation of NH_4^+-N (Chen et al. 2021). The observed pH values of the biochar at the zero-charge point (pH_{pzc}) exceeded the theoretical values, as shown in Table 1. This suggests that the biochar surface possessed a negative charge, which is conducive to the NH_4^+ ions electrostatic adsorption.

The existence of ordered structures and aromatic carbons in RB, RB-H_2O_2, RB-$KMnO_4$, and RB-NaOH was confirmed by Raman spectroscopy, as illustrated in Fig. 2. Spectroscopic analysis provided evidence of the structural integrity and chemical composition of these materials, underscoring the presence of aromatic carbon configurations. All the biochars under investigation displayed two primary non-graphitic carbon bands, the G band at 1579 cm^{-1} and the D band at 1326 cm^{-1}, as depicted in Fig. 2a. The G-band represents the ideal graphite lattice, while the D-band represents the disordered graphite lattice. The presence of these G and D bands suggests the existence of sp2 bonded carbon within the biochar, as reported by Hossain et al. (2018). Notably, the ID/IG ratio of the modified biochar decreased significantly, implying a more structured carbon arrangement (Tripathy et al. 2021).

Thermogravimetric analysis was conducted to evaluate the thermal steadiness and weight loss action of biochar under an N_2 atmosphere from 30 to 1000 ℃, as depicted in Fig. 3. Primarily, the evaporation of water involved van der Waals forces of attraction between molecules, and adsorption on the MB surface resulted in the loss of weight up to a temperature of 110 ℃ (Tripathy et al. 2021). Figure 3 indicates that there were three stages of weight loss for the unmodified biochar, whereas only two stages of mass loss were observed in the modified biochar. Thus, the thermal stability of RB-$KMnO_4$ was significantly improved.

The BET analysis results for RB and MB are presented in Table 2. Notably, the micropore area, BET surface area, and pore size of RB-$KMnO_4$ were higher than those of MB. All the biochars exhibited microporosity (pores within the scope of 2–16 nm according to Fig. 4a). The mean pore diameter fluctuated within a range of 3.72–4.54 nm. The nitrogen adsorption–desorption isotherms of biochar exhibited characteristics consistent with a Type II isotherm (Fig. 4b), which indicated that a physical adsorption process occurred on nonporous or macroporous solid surfaces, a phenomenon pertinent to the field of soil biophysics. The isotherm displayed a distinct H4 hysteresis loop, implying that the modified biochar had narrow slit-like pores and an incomplete pore network (Gopinath et al. 2021).

Furthermore, the N_2 adsorption–desorption isotherm of RB-$KMnO_4$ was substantially higher than those of the other treatments, implying the effectiveness of modification with $KMnO_4$. However, the N_2 adsorption–desorption isotherm of RB-NaOH was the lowest. One extremely possible reason is that under high concentration sodium hydroxide (> 2 mol L^{-1}) modification conditions, sodium carbonate (Na_2CO_3) crystals are formed on the surface of RB-NaOH, which can hinder the formation of pores or block the original pores (Table 2) (Hu et al. 2018). This implies that when using high concentrations of modifiers for modification, we also need to coordinate appropriate reaction conditions to efficiently exert the effect of the modifier.

3.1.3 FTIR analysis

Characterization of the infrared spectra and investigation of the surface functional groups of the biochars were conducted using FTIR, as depicted in Fig. 5. Upon alteration, an increase in the intensity of the O–H tensile vibration peak was observed at approximately 3400 cm^{-1}. The peak within the scope

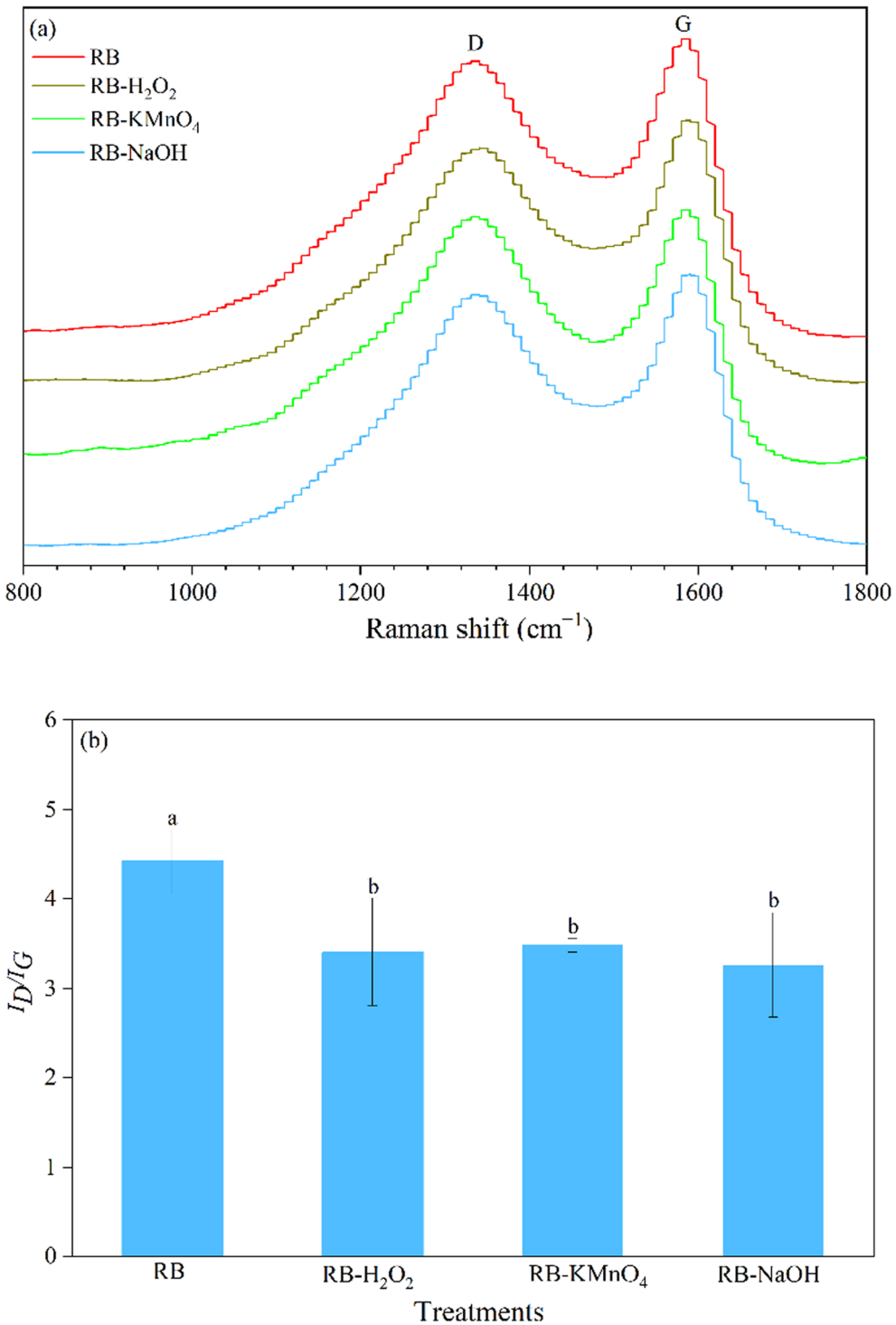

Fig. 2 Raman analysis of RB, RB-H_2O_2, RB-NaOH and RB-$KMnO_4$. Different letters indicate a significant difference ($P < 0.05$). RB means residue biochar; RB-H_2O_2 means residue biochar modified by H_2O_2; RB-NaOH means residue biochar modified by NaOH; RB-$KMnO_4$ means residue biochar modified by $KMnO_4$

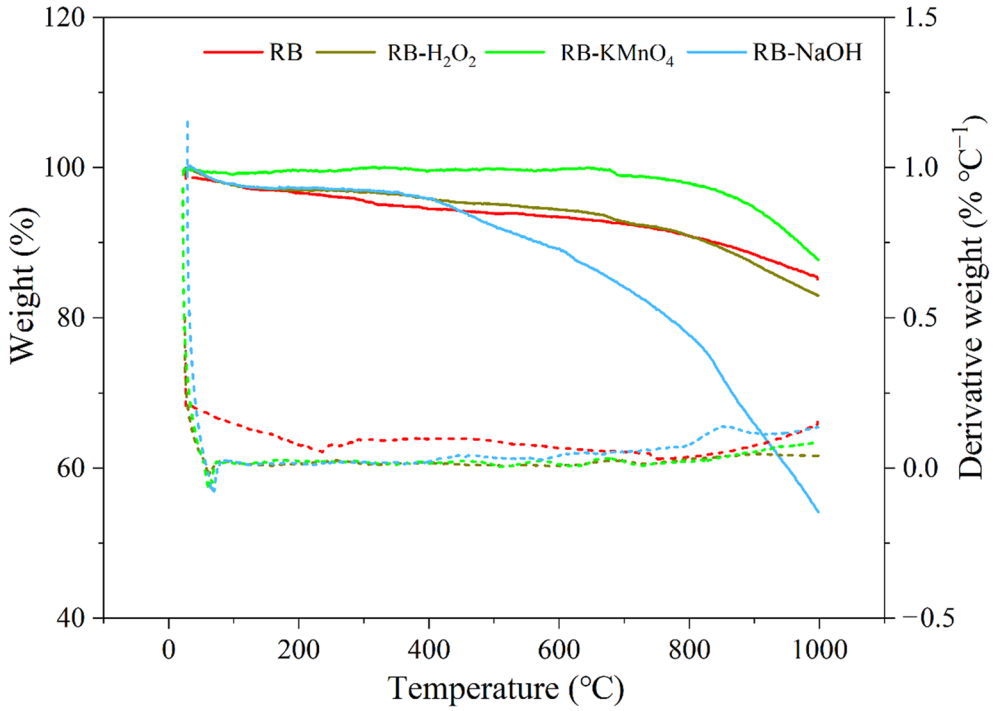

Fig. 3 Thermogravimetric analysis of RB, RB-H_2O_2, RB-NaOH and RB-$KMnO_4$. RB means residue biochar; RB-H_2O_2 means residue biochar modified by H_2O_2; RB-NaOH means residue biochar modified by NaOH; RB-$KMnO_4$ means residue biochar modified by $KMnO_4$

Table 2 Pore structure of biochars

Biochar	S_{BET}[a] ($m^2\ g^{-1}$)	S_{Micro}[b] ($m^2\ g^{-1}$)	S_{Ext}[c] ($m^2\ g^{-1}$)	V_{Tot}[d] ($cm^3\ g^{-1}$)	V_{Micro}[e] ($cm^3\ g^{-1}$)	V_{Meso}[f] ($cm^3\ g^{-1}$)	D_{Tot}[g] (nm)
RB	236.80	202.16	34.64	0.1164	0.0769	0.0395	3.72
RB-H_2O_2	256.68	238.40	18.28	0.1144	0.0897	0.0247	4.02
RB-$KMnO_4$	301.69	266.25	35.45	0.1524	0.1012	0.0512	4.05
RB-NaOH	199.00	180.33	18.67	0.1064	0.0673	0.0391	4.54

[a] specific surface area calculated using the Brunauer-Emmet-Teller (BET) method

[b] t-plot micropore area

[c] t-plot external surface area

[d] single point adsorption total pore volume of pores at P/P0 ≈ 0.994

[e] t-plot micropore volume

[f] $V_{Meso} = V_{Tot} - V_{Micro}$, mesopore volume

[g] average pore diameter of total pore

of 1612–1585 cm^{-1} was caused by the aromatic carbon structure, specifically the C=C and C=O bonds. Additionally, the out-of-plane bending vibration and stretching of C–H were enhanced by the two distinct bands at 801 and 462 cm^{-1}. The relative content of the C=C functional groups of RB-$KMnO_4$ was 88.12%, which was higher than those of the other biochars, as shown in Table 3. The peak value of the asymmetric stretching vibration of aromatic C–O–C (C–O stretching vibration of easily degradable carbohydrates such as polysaccharides) at 1085 cm^{-1} was significantly enhanced, particularly in RB-NaOH. This suggests an increase in the aromaticity of RB-NaOH, which enhances the adsorptive characteristics of the biochar. The relative content of C–O–C functional groups in RB-H_2O_2 is intermediate. Furthermore, the stretching vibration peak of Fe–O at 586 cm^{-1} in RB-NaOH suggests an increased capacity for ammonium adsorption.

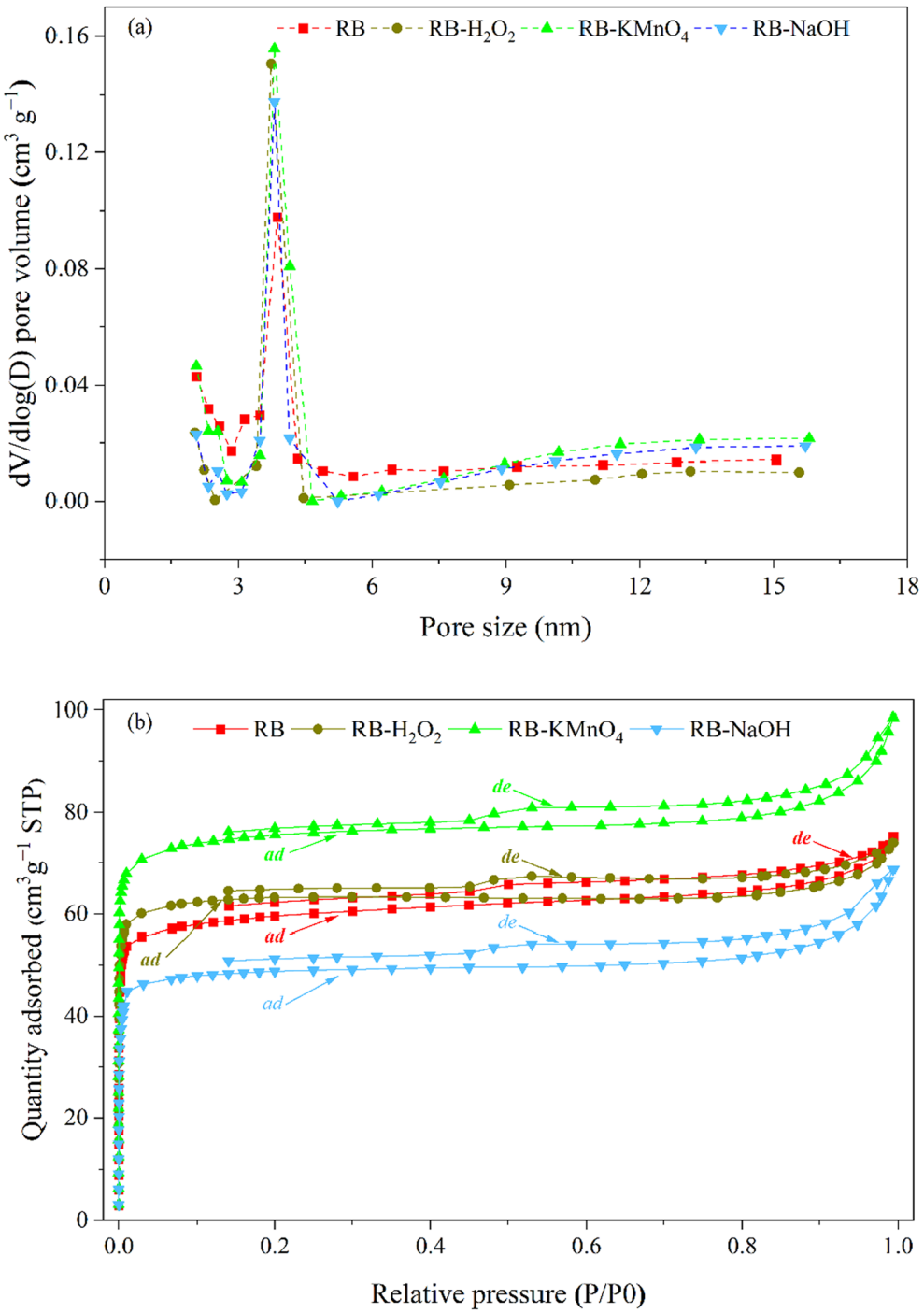

Fig. 4 Pore size distribution (**a**) and quantity adsorbed (**b**) of RB, RB-H_2O_2, RB-NaOH and RB-$KMnO_4$. RB means residue biochar; RB-H_2O_2 means residue biochar modified by H_2O_2; RB-NaOH means residue biochar modified by NaOH; RB-$KMnO_4$ means residue biochar modified by $KMnO_4$

3.2 Adsorption performance

3.2.1 Adsorptioon before and after modification

Figure 6 shows the adsorption capabilities of both unaltered and chemically enhanced biochars for NH_4^+-N across a spectrum of NH_4^+-N concentrations. The modified biochar exhibited superior adsorption performance compared to the unmodified biochar in solutions with higher NH_4^+-N concentrations (> 20 mg L^{-1}), especially for RB-$KMnO_4$. In the 150 mg L^{-1}

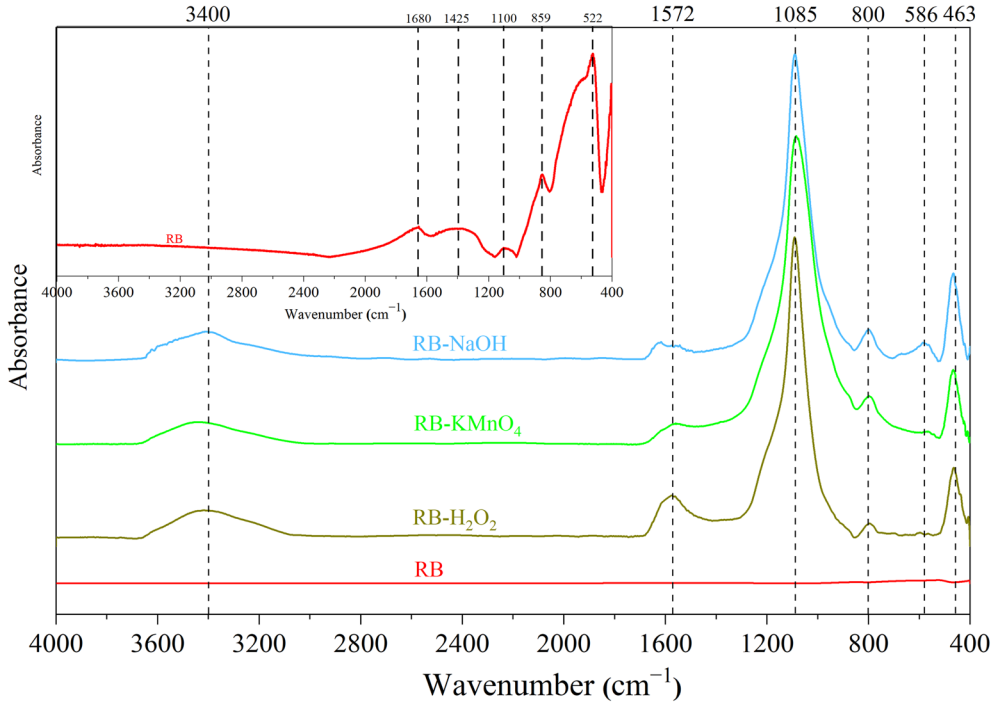

Fig. 5 The functional groups of RB, RB-H_2O_2, RB-NaOH and RB-$KMnO_4$ under FTIR spectra. RB means residue biochar; RB-H_2O_2 means residue biochar modified by H_2O_2; RB-NaOH means residue biochar modified by NaOH; RB-$KMnO_4$ means residue biochar modified by $KMnO_4$

Table 3 The relative content functional groups (%)

Functional groups	eV	RB	RB-H_2O_2	RB-$KMnO_4$	RB-NaOH
C=C(C–C)	284.49	86.57	75.39	88.12	66.99
C–O	285.69	12.95	24.61	11.88	33.01
C=O	286.99	0.48	0	0	0
–COOH	288.89	0	0	0	0

eV binding energy

NH_4^+-N solution, the adsorbance of RB-H_2O_2, RB-$KMnO_4$, and RB-NaOH increased 2.99, 3.99, and 3.21 times compared with that of RB. This might be caused by the increase in the pore volume and surface area of RB-$KMnO_4$, which provides more adsorption sites (Table 1). In addition, an increase in the C=C functional group content further increased the ammonium adsorption capacity (Fig. 5).

3.2.2 Adsorption kinetics

The kinetic behavior of NH_4^+-N adsorption onto both the modified and unmodified biochars was investigated, as illustrated by the corresponding fitted curves in Fig. 7. A detailed summary of the fitting results is provided in Table 4. The simulation results indicated that the NH_4^+-N adsorption process on both biochar types was characterized by an initial rapid increase within

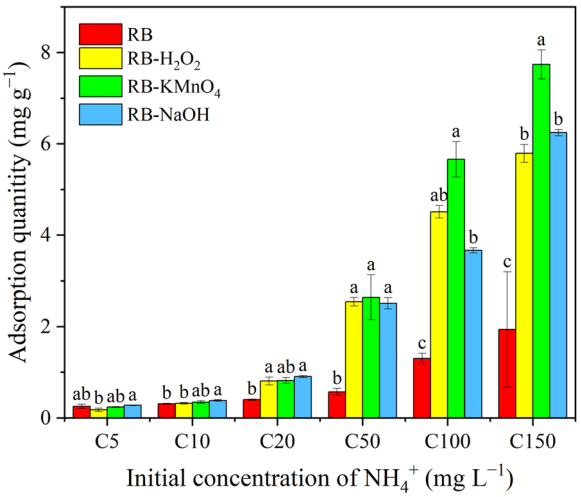

Fig. 6 Influence of initial concentration on RB, RB-H_2O_2, RB-NaOH and RB-$KMnO_4$ adsorption capacity. RB means residue biochar; RB-H_2O_2 means residue biochar modified by H_2O_2; RB-NaOH means residue biochar modified by NaOH; RB-$KMnO_4$ means residue biochar modified by $KMnO_4$

the first 1.5 h, followed by a more gradual increase in adsorption capacity until saturation was achieved at approximately 2 h. Notably, the adsorption capacity of RB-$KMnO_4$ surpassed that of the other chars. The pseudo-first and second-order kinetic models (Fig. 7a,

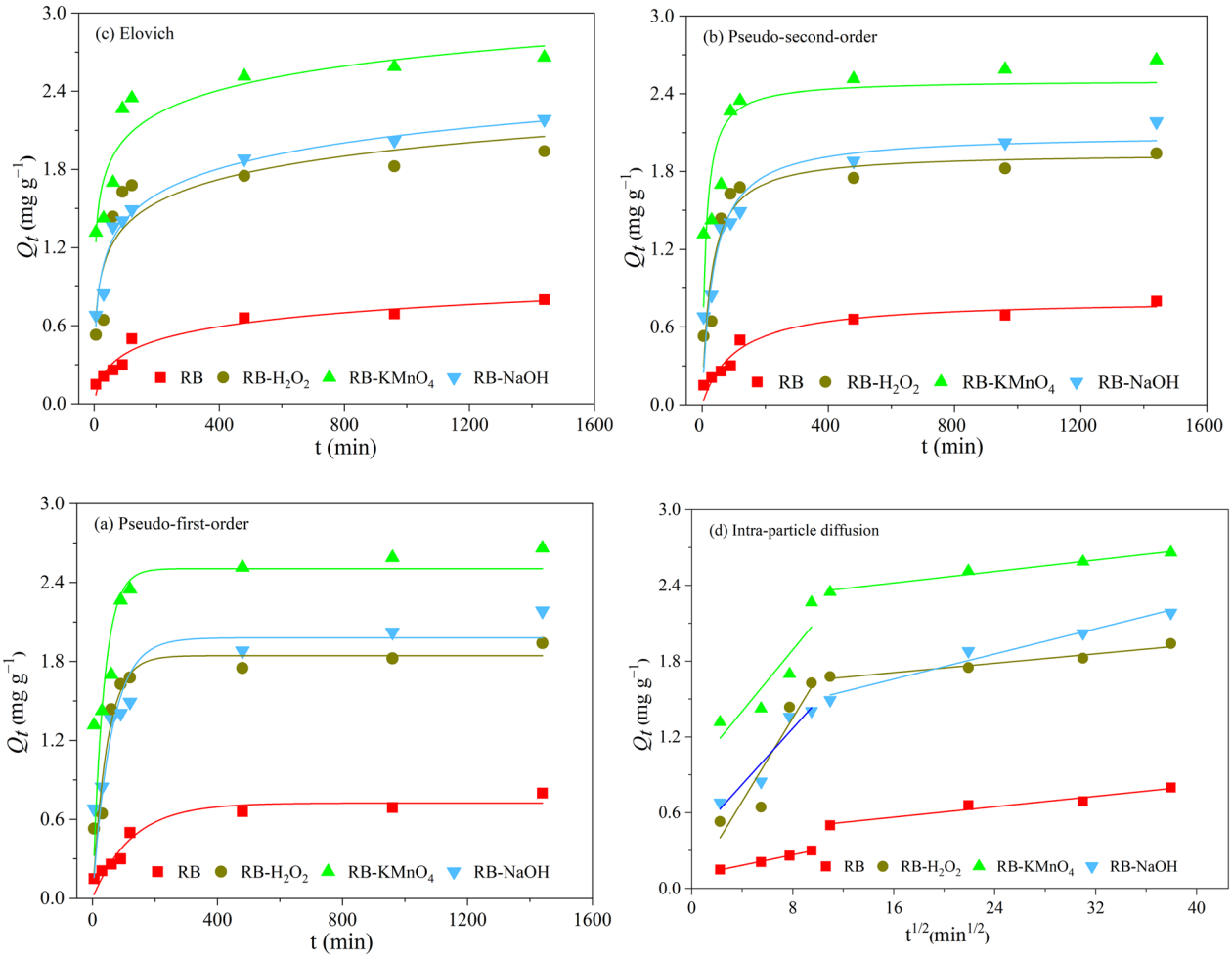

Fig. 7 Adsorption kinetics of NH_4^+-N on RB (**a**), RB-H_2O_2 (**b**), RB-NaOH (**c**) and RB-$KMnO_4$ (**d**). Q_t means the adsorption quantity at a certain time (mg g^{-1}). RB means residue biochar; RB-H_2O_2 means residue biochar modified by H_2O_2; RB-NaOH means residue biochar modified by NaOH; RB-$KMnO_4$ means residue biochar modified by $KMnO_4$

Table 4 Adsorption kinetics parameters of modified biochar

Kinetic models	Parameters	RB	RB-H_2O_2	RB-$KMnO_4$	RB-NaOH
Pseudo-first-order	k_1 (min^{-1})	0.0080	0.0215	0.0279	0.0166
	Qe (mg g^{-1})	0.7241	1.8440	2.5054	1.9794
	R^2	0.9183	0.9010	0.4461	0.7973
Pseudo-second-order	k_2 (min^{-1})	0.0115	0.0183	0.0346	0.0131
	Qe (mg g^{-1})	0.8140	1.9454	2.5053	2.0894
	R^2	0.9339	0.8815	0.6689	0.8804
Elovich	α (mg g^{-1} min^{-1})	0.0167	0.5185	5.6783	0.3972
	β (mg g^{-1})	6.3670	3.8836	3.7587	3.5015
	R^2	0.9403	0.8035	0.8629	0.9647
Intra-particle diffusion	K_{p1}(mg g^{-1} min$^{-1/2}$)	0.0207	0.1648	0.1216	0.1108
	C_1 (mg g^{-1})	0.1011	0.0320	0.9180	0.3820
	R^2	0.9972	0.8710	0.8057	0.9044
	k_{P2} (mg g^{-1} min$^{-1/2}$)	0.0103	0.0093	0.0113	0.0250
	C_2 (mg g^{-1})	0.3993	1.5607	2.2390	1.2594
	R^2	0.9506	0.9521	0.9802	0.9705

b), as indicated by their lower R^2 values, were insufficient to accurately characterize the adsorption process of NH_4^+-N, especially in the case of RB-$KMnO_4$ ($R^2 < 0.66$) and RB-H_2O_2 ($R^2 < 0.88$).

The NH_4^+-N adsorption process by both modified and unmodified biochars can be delineated into two distinct phases, as per the intra-particle diffusion kinetic equation (Fig. 7d). This equation, which exhibited a superior R^2 value (> 0.95), offered a more accurate depiction of NH_4^+-N adsorption on modified biochar when juxtaposed with other kinetic models. The fitting parameters R^2 for the intra-particle diffusion kinetics equation were 0.9972 (RB, first stage), 0.9521 (RB-H_2O_2, second stage), 0.9802 (RB-$KMnO_4$, second stage), and 0.9705 (RB-NaOH, second stage) (Fig. 7d). These values were significantly higher than those obtained from other equations, thereby underscoring the efficacy of the diffusion kinetics equation within the particles in describing the NH_4^+-N adsorption process.

In Fig. 7d, the first stage of the intra-particle diffusion model is attributed to rapid attachment of ammonium ions to the outer surface and macropores of biochar after undergoing liquid film diffusion. On the one hand, the concentration of NH_4^+-N in the solution is higher, which increases the contact probability between ammonium ion and biochar material, providing conditions for the increase of adsorption capacity. On the other hand, this process is also influenced by the adsorption sites of ammonium ions on the particle surface (Hai et al. 2025; Skic et al. 2024). As the process transitioned to the subsequent gradual adsorption phase, the solute concentration decreased, causing an increase in the diffusion resistance within the carbonaceous material. The adsorption sites on the surface of biochar tend to be saturated gradually, and the concentration difference of NH_4^+-N in the liquid film on the surface of biochar material decreases gradually, resulting in the equilibrium state of adsorption rate and desorption rate. The following was the second stage—slow diffusion of ammonium ions within the micropores of biochar. Thus, the curve exhibits a relatively flat state. The intra-particle diffusion is influenced by the pore structure of biochar. Its pore size distribution and specific surface area both affect the migration rate (Ai et al. 2024; Kang et al. 2024). The above diffusion process well explained the reason why the intraparticle diffusion model did not pass through the origin, which further illustrated that the potential kinetic mechanism of adsorption was a multifaceted process, including liquid film diffusion, surface adsorption, and intra-particle diffusion (Jiang et al. 2019; Wu et al. 2014). This intricate mechanism integrates various aspects of material interactions, demonstrating the multifaceted nature of adsorption kinetics.

The intra particle diffusion model effectively explained the high adsorption capacity of biochar modified with $KMnO_4$. The higher C_2 (2.2390 mg g^{-1}) of potassium permanganate meant that more NH_4^+ reached the surface of the particles. Then, the richer, deeper, and rougher pores of RB-$KMnO_4$ created conditions for its higher intraparticle diffusion rate and adsorption capacity (Fig. 1d and Table 2). Moreover, under the condition of consistent solution flow rate and temperature, the higher pH of RB-$KMnO_4$ solution also provided advantages for the liquid film diffusion of ammonium ions (Table 1). Because at high pH values, ammonium ions mainly exist in a free state and are more easily adsorbed (Lu et al. 2024). This further illustrates that modified biochar materials exhibit differences in adsorption kinetics during the adsorption process by comprehensively affecting the liquid film diffusion process, surface adsorption process, and intra particle diffusion process.

3.2.3 Adsorption isotherm

The fitting curve of the adsorption isotherm of NH_4^+-N on the modified biochar is shown in Fig. 8, indicating an increasing trend in the adsorption capacity of NH_4^+-N. Table 5 further delineates the association parameters (R^2) for the Langmuir model, with values of 0.9920 (RB-H_2O_2), 0.9863 (RB-$KMnO_4$), and 0.9690 (RB-NaOH), all of which surpassed those of the Freundlich model. This suggests that isothermal NH_4^+-N adsorption onto biochar predominantly adheres to the Langmuir isotherm model (Lingamdinne et al. 2020). Consequently, the primary mechanism underlying ammonium adsorption by MB was inferred to be monolayer adsorption on a highly homogeneous surface.

The adsorption process is predominantly monolayer in nature and is characterized by chemisorption (Li et al. 2017). For RB, the fitting coefficients R^2 were greater for the Freundlich model than for the Langmuir model. Additionally, the results indicate that the Langmuir isotherm model more accurately describes the adsorption characteristics of MB for NH_4^+-N. The equilibrium constant (K_L) of Langmuir equation is in the range of $0 < K_L < 1$, indicating that adsorption is not a spontaneous process. In addition, K_L represents the adsorption capacity of biochar for NH_4^+-N. In this study, the K_L of RB-H_2O_2 was higher than that of other biochar materials, indicating that RB-H_2O_2 had the highest affinity for NH_4^+- N in solution.

Compared with previous studies, the fitting results of the Langmuir model demonstrated the significant adsorption advantage of modified biochar from biogas residue, with the adsorption capacity increasing from 9.08 mg g^{-1} to 13.93–68.15 mg g^{-1}. Wang et al. (2023) modified chicken manure biochar with $FeCl_3$, and

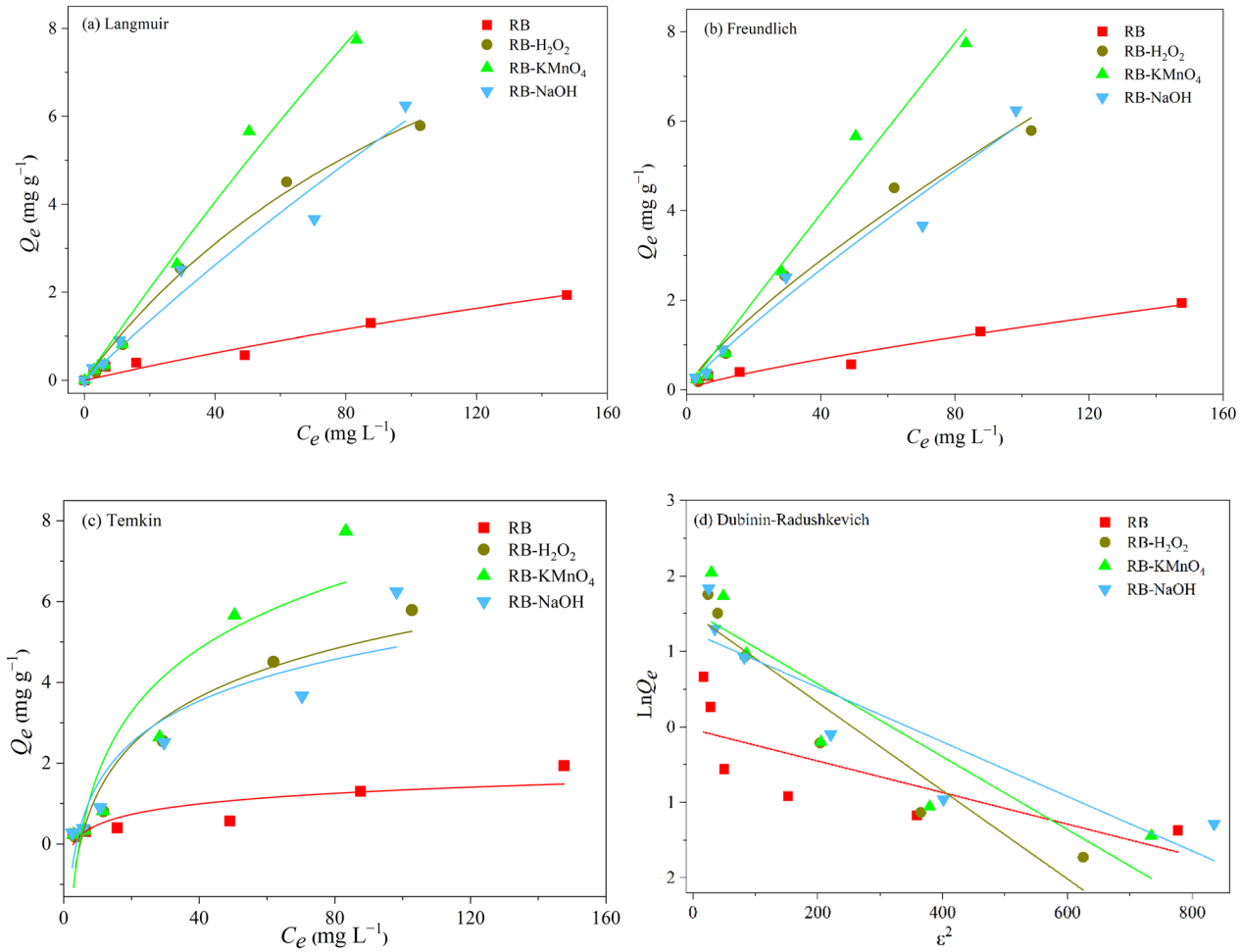

Fig. 8 Adsorption isotherms of NH_4^+-N on RB (**a**), RB-H_2O_2 (**b**), RB-NaOH (**c**) and RB-$KMnO_4$ (**d**). Q_e means the equilibrium adsorption capacity (mg g^{-1}). RB means residue biochar; RB-H_2O_2 means residue biochar modified by H_2O_2; RB-NaOH means residue biochar modified by NaOH; RB-$KMnO_4$ means residue biochar modified by $KMnO_4$

Table 5 Adsorption isotherm parameters for the 3 types of modified biochar

Isotherm models	Parameters	RB	RB-H_2O_2	RB-$KMnO_4$	RB-NaOH
Langmuir	Q_m (mg g^{-1})	9.0781	13.9269	68.1534	41.0008
	K_L (L mg^{-1})	0.0018	0.0072	0.0016	0.0017
	R^2	0.9391	0.9920	0.9863	0.9690
Freundlich	K_F ($mg^{(1-1/1n)}$ $L^{-1/n}$ g^{-1})	0.0388	0.1585	0.1067	0.1093
	1/n	0.7788	0.7872	0.9780	0.8681
	R^2	0.9514	0.9777	0.9824	0.9678
Temkin	b (J mol^{-1})	6600.7589	1437.1208	1101.0007	1666.4864
	K_T (L mg^{-1})	0.3526	0.2061	0.2140	0.2701
	R^2	0.7438	0.9397	0.8585	0.8531
Dubinin-Radushkevich	Q_m (mg g^{-1})	0.9672	4.4540	4.6338	3.4812
	K_{DR} (mol^2 kJ^{-2})	0.0021	0.0058	0.0048	0.0036
	E (kJ mol^{-1})	15.4672	9.2529	10.1850	11.7688
	R^2	0.5799	0.9104	0.8039	0.7997

the maximum adsorption capacity of NH_4^+ reached 55.29 mg g^{-1}. Song et al. (2024) modified pig manure biochar with different acid–base modification methods, and the adsorption capacity of ammonium nitrogen in neutral environment was 2.53 mg g^{-1}. It may be inferred that the adsorption performance of different biochar materials modified with different modifiers varies greatly. The types of raw materials used in the preparation of biochar, the conditions for biochar preparation, and the methods of biochar modification are all important factors that affect the porosity, specific surface area, and functional group expression of modified biochar. (Chen et al. 2021; Halder et al. 2023). The influences of solution pH, competitive ions, and initial NH_4^+-N concentration on the NH_4^+-N adsorption capacity of modified biochar are further analyzed and discussed in the Supplementary Materials. Therefore, in the modification process, it is also necessary to choose suitable modifiers to achieve better adsorption performance.

3.3 Mechanism of NH_4^+-N adsorption on altered biochar

Compared with unmodified biochar, the adsorption capacity of MB was significantly enhanced. However, the mechanisms underlying the improved adsorption performance varied among the three types of modified biochar (Fig. 9). In the above, we elucidated the adsorption advantages of RB-$KMnO_4$ from the perspective of the intra particle diffusion model. The enhanced adsorption capacity was primarily attributed to the improved pore structure of biochar, which was characterized by a significant increase in both pore volume and specific surface area (Table 2). Oxidation treatment can create additional micropores and mesopores on the biochar surface, thereby increasing the specific surface area and providing more adsorption sites (Chen et al. 2022). However, modification of biochar using another oxidizing agent, H_2O_2, only resulted in a minor improvement in its adsorption performance. Unlike $KMnO_4$, the oxidation by H_2O_2 did not significantly enhance the pore structure of biochar but instead led to a notable increase in the –C–O functional groups on the surface of RB-H_2O_2 (Table 2), accompanied by minor increases in –OH and –COOH functional groups (Fig. 5). These oxygen-containing functional groups can elevate the negative charge density on the biochar surface, thereby enhancing the electrostatic attraction to cations such as NH_4^+ (Liu et al. 2024a, b). The adsorption mechanism of RB-NaOH was similar to that of RB-H_2O_2, both of which significantly increased

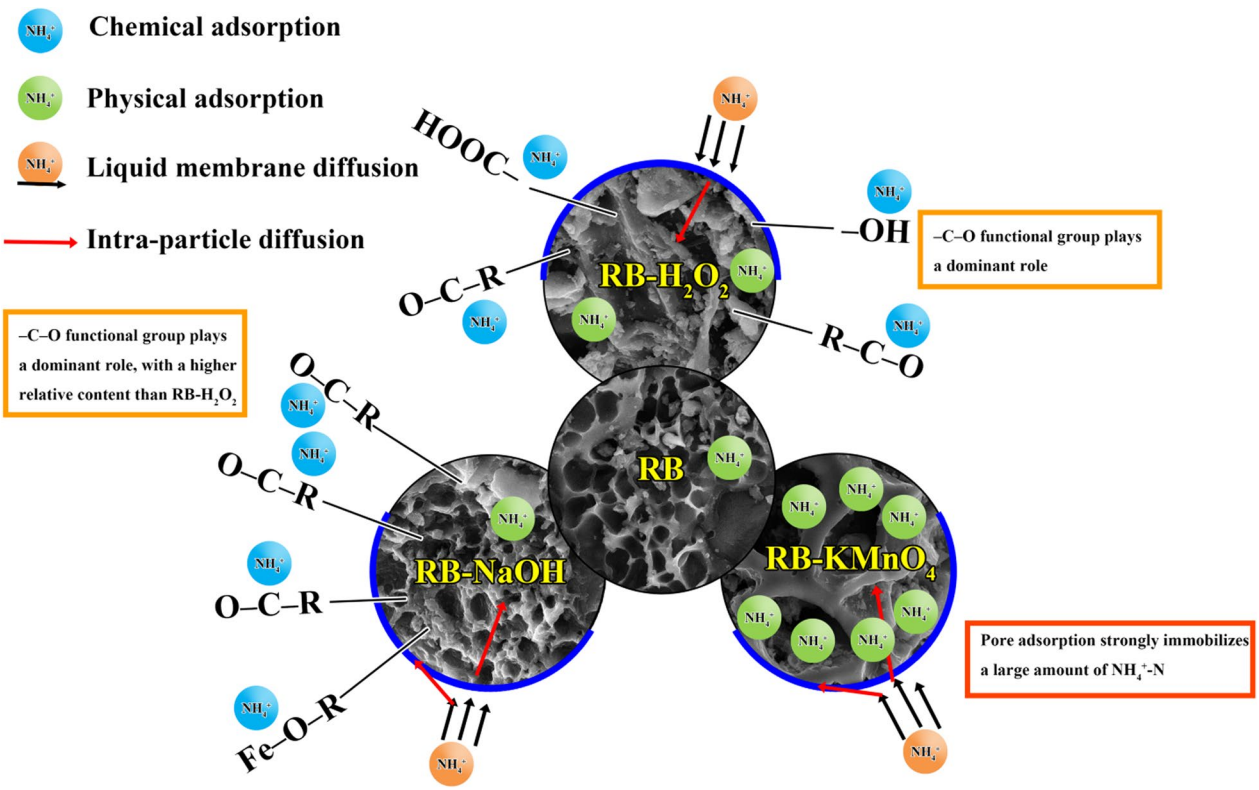

Fig. 9 Adsorption mechanisms of RB-H_2O_2, RB-NaOH and RB-$KMnO_4$. RB means residue biochar; RB-H_2O_2 means residue biochar modified by H_2O_2; RB-NaOH means residue biochar modified by NaOH; RB-$KMnO_4$ means residue biochar modified by $KMnO_4$

the –C–O functional groups on the biochar surface (Table 3). However, RB-NaOH also slightly introduced Fe–O functional groups (Fig. 5). Although RB-NaOH exhibited relatively lower specific surface area and total pore volume, its adsorption capacity surpassed that of RB-H_2O_2 (Table 5 and Fig. 6). This discrepancy can be attributed to the fact that NaOH modification was more effective than H_2O_2 modification in increasing the relative content of –C–O functional groups on the biochar surface (Table 3). However, neither modification strategy surpassed the adsorption performance of RB-$KMnO_4$, indicating that pore adsorption is more advantageous than surface functional group adsorption for NH_4^+-N. There are three factors attributed to this superiority. Firstly, the increased internal surface area, particularly the presence of micropores and mesopores, provides a larger adsorption surface, allowing more ammonium ions to enter and be immobilized within these pores (Cai et al. 2022). Secondly, the diffusion and accommodation mechanism play a crucial role. Once ammonium ions enter the pores of biochar, they are less likely to desorb due to spatial confinement effects. This intrinsic trapping effect significantly enhances adsorption efficiency. In contrast, although surface functional groups can capture ammonium ions through chemical bonding, their capacity is limited (Joshi et al. 2023). Thirdly, competitive adsorption sites pose a challenge for surface functional groups. When multiple pollutants or ions coexist, surface functional groups may engage in competitive adsorption, reducing the effective adsorption capacity for specific targets such as ammonium ions. In contrast, pore structures are less affected by competition because they primarily rely on physical adsorption processes rather than chemical interactions (Sumaraj et al. 2020). Besides, it is also important to consider the potential for $KMnO_4$ to react with organic components in biochar, forming more stable complexes that enhance biochar stability and adsorption efficiency (Shang et al. 2020).

4 Conclusion

As the concentration of NH_4^+-N solution increased, the MB exhibited a more pronounced adsorption advantage. The maximum adsorption capacities of these three MB were 13.93, 41.00, and 68.15 mg g^{-1}, respectively, from the Langmuir isotherm model. Ammonium adsorption on the MB surfaces was affected by surface adsorption, liquid membrane diffusion, and intra-particle diffusion. The adsorption mechanisms of ammonium ions by different MB were distinct. Relative to RB, the modification with $KMnO_4$ enhanced the specific surface area and pore volume of biochar, thereby optimizing its pore structure. This led to a significant increase in the number of active sites on RB-$KMnO_4$, which in turn enhanced its adsorption capacity for NH_4^+-N. The adsorption of NH_4^+-N by RB-NaOH primarily relied on functional group interactions, including –C–O and Fe–O, while RB-H_2O_2 adsorbed NH_4^+-N mainly through –C–O functional groups, with weaker contributions from –OH and –COOH. The modified biochar tended to exhibit more efficient adsorption performance under neutral pH conditions, with lower concentrations of competitive ions and higher concentrations of NH_4^+-N solution. Overall, biochars modified with $KMnO_4$, H_2O_2, and NaOH exhibited superior performance in adsorbing ammonium nitrogen. Among these, RB-$KMnO_4$ demonstrated the highest adsorption efficiency, with pore-based adsorption playing a dominant role over functional group-based adsorption. These findings highlight the critical role of pore structure optimization in enhancing the adsorption capacity of biochar for ammonium nitrogen.

Supplementary Information

The online version contains supplementary material available at https://doi.org/10.1007/s42773-025-00500-z.

Supplementary material 1.

Acknowledgements
Not applicable.

Author contributions
Ping Cong: investigation, data analysis, original draft preparation; Shuhui Song: conceptualization, supervision and methodology; Yanmei Zhu: supervision, data curation; Xinwei Ji and Shuai Liu: writing-review and editing; Shuai Kuang: writing-original draft preparation; Yanli Xu and Qiuqiang Hou: project administration; Xuebo Zheng: data analysis, supervision and methodology; Wenjing Song: data curation and supervision.

Funding
This study was supported by the National Natural Science Foundation of China (32301969; 31901195), Shandong Provincial Natural Science Foundation (ZR2024MC159), the Agricultural Science and Technology Innovation Program of the Chinese Academy of Agricultural Sciences (ASTIP-TRIC03), and Yunnan Branch of China National Tobacco Corporation (2024530000241031).

Data availability
The datasets generated during the current study are available from the corresponding author on reasonable request.

Declarations

Competing interests
The authors have no competing interests to declare that are relevant to the content of this article.

Author details
[1]Key Laboratory of Tobacco Biology and Processing, Ministry of Agriculture and Rural Affairs, Tobacco Research Institute of Chinese Academy of Agricultural Sciences, Qingdao 266101, China. [2]Key Laboratory of Tropical Crops Nutrition of Hainan Province, Ministry of Agriculture and Rural Affairs, South Subtropical Crops Research Institute, Chinese Academy of Tropical Agricultural Sciences, Zhanjiang 524091, China. [3]Honghe Prefecture Branch of Yunnan Tobacco Company, Mile, China.

Received: 17 October 2024 Revised: 11 July 2025 Accepted: 21 July 2025
Published online: 25 August 2025

References

Ai ZJ, Luo S, Xu ZY, Cao JB, Leng LJ, Li HL (2024) Prediction and optimization design of porous structure properties of biomass-derived biochar using machine learning methods. Energy 313:133707. https://doi.org/10.1016/j.energy.2024.133707

Cai GJ, Ye ZL (2022) Concentration-dependent adsorption behaviors and mechanisms for ammonium and phosphate removal by optimized Mg-impregnated biochar. J Clean Prod 349:131453. https://doi.org/10.1016/j.jclepro.2022.131453

Cao X, Harris W (2010) Properties of dairy manure derived biochar pertinent to its potential use in remediation. Bioresour Technol J 101:5222–5228. https://doi.org/10.1051/matecconf/20166707006

Chen M, Wang F, Zhang DL, Yi WM, Liu Y (2021) Effects of acid modification on the structure and adsorption NH_4^+-N properties of biochar. Renewable Energy 169:1343–1350. https://doi.org/10.1016/j.renene.2021.01.098

Chen AX, Zhang YX, Wei X, Pang JJ, Hu RR, Guan JJ (2022) Preparation of in-situ nitrogen-doped lignin-based porous carbon and its efficient adsorption of chloramphenicol in water. Environ Sci Pollut Res 29(49):74306–74318. https://doi.org/10.1007/s11356-022-20045-z

Cong P, Song SH, Song WJ, Dong JX, Zheng XB (2022) Biochars prepared from biogas residues: Temperature is a crucial factor that determines their physicochemical properties. Biomass Convers Biorefin 14(12):12843–12856. https://doi.org/10.1007/s13399-022-03229-y

Duygan BDÖ, Udert KM, Remmele A, McArdell CS (2021) Removal of pharmaceuticals from human urine during storage, aerobic biological treatment, and activated carbon adsorption to produce a safe fertilizer. Resour Conserv Recycl J 166:105341. https://doi.org/10.1016/j.resconrec.2020.105341

Feng SJ, Xu W, Wang MG, Zhao YH, Strokal M, Kroeze C, Ma L, Zhang F (2023a) Elevated ammonia emission neutralized alleviation of nitrogen deposition to water pollution in China. EGU General Assembly Conference Abstracts P: 13672. https://doi.org/10.1111/nph.12494

Feng YX, Jin CH, Xue Q, Liu YR, Liu NN, Li ZQ, Liu SW, Huang YY (2023b) Potassium permanganate and sodium silicate co-modified bamboo charcoal for efficient treatment of ammonia nitrogen pollution in rare earth mines: performance and mechanism. Water Air Soil Pollut 234(2):109. https://doi.org/10.1007/s11270-022-06020-x

Gopinath A, Divyapriya G, Srivastava V, Laiju AR, Nidheesh P, Kumar MS (2021) Conversion of sewage sludge into biochar: A potential resource in water and wastewater treatment. Environ Res J 194:110656. https://doi.org/10.1016/j.envres.2020.110656

Gsior D, Tic WJ (2016) Biochar application in the mercury ions adsorption from aqueous solutions. Environ Socio-Econ Stud J 16(440):803–818

Hai NT, Hoang-Minh T, Hieu DT, Hien PT, Dung LV, Hoai TT, Dong BV, Ha NTH (2025) Adsorption characteristics of ammonium on activated biochar synthesized from sugarcane waste: batch and column studies. Biomass Convers Biorefin. https://doi.org/10.1007/s13399-025-06579-5

Hailegnaw NS, Mercl F, Pračke K, Száková J, Tlustoš P (2019) High temperature-produced biochar can be efficient in nitrate loss prevention and carbon sequestration. Geoderma 338:48–55. https://doi.org/10.1016/j.geoderma.2018.11.006

Halder P, Marzbali MH, Patel S, Short G, Surapaneni A, Gupta R, Shah K (2023) Ammonium nitrogen (NH_4^+-N) recovery from synthetic wastewater using biosolids-derived biochar. Bioresour Technol Rep 23:101592. https://doi.org/10.1016/j.biteb.2023.101592

Hossain MZ, Wu W, Xu WZ, Chowdhury MB, Jhawar AK, Machin D, Charpentier PA (2018) High-surface-area mesoporous activated carbon from hemp bast fiber using hydrothermal processing. Chimia J 4(3):38. https://doi.org/10.3390/c4030038

Hou J, Huang L, Yang ZM, Zhao YQ, Deng CR, Chen YC, Li X (2016) Adsorption of ammonium on biochar prepared from giant reed. Environ Sci Pollut Res J 23:19107–19115. https://doi.org/10.1007/s11356-016-7084-4

Hu XL, Xue YW, Long L, Zhang KJ (2018) Characteristics and batch experiments of acid- and alkali-modified corncob biomass for nitrate removal from aqueous solution. Environ Sci Pollut Res 25(20):19932–19940. https://doi.org/10.1007/s11356-018-2198-5

Jiang YH, Li AY, Deng H, Ye CH, Wu YQ, Linmu YD, Hang HL (2019) Characteristics of nitrogen and phosphorus adsorption by Mg-loaded biochar from different feedstocks. Bioresour Technol J 276:183–189. https://doi.org/10.1016/j.biortech.2018.12.079

Jiang SF, Hu ZY, Chen S, Hao HC, Jiang H (2024) Green synthesis of Fe-anchored N-doped biochar with highly active FeNx catalytic sites for electrochemical nitrate reduction. J Environ Chem Eng 12(1):111915. https://doi.org/10.1016/j.jece.2024.111915

Joshi M, Bhatt D, Srivastava A (2023) Enhanced adsorption efficiency through biochar modification: a comprehensive review. Ind Eng Chem Res 62(35):13748–13761. https://doi.org/10.1021/acs.iecr.3c02368

Kang YG, Park DG, Lee JY, Choi J, Kim JH, Kim JH, Yun YU, Oh TK (2024) Ammonium capture kinetic, capacity, and prospect of rice husk biochar produced by different pyrolysis conditions. Sci Rep 14(1):1–14. https://doi.org/10.1038/s41598-024-80873-6

Kaur N, Bhardwaj P, Singh G, Arya SK (2021) Applicative insights on nascent role of biochar production, tailoring and immobilization in enzyme industry -a review. Process Biochem J 107(8):153–163. https://doi.org/10.1016/j.procbio.2021.05.017

Li HQ, Hu JT, Meng Y, Su JH, Wang XJ (2017) An investigation into the rapid removal of tetracycline using multilayered graphene-phase biochar derived from waste chicken feather. Sci Total Environ J 603:39–48. https://doi.org/10.1016/j.scitotenv.2017.06.006

Li RH, Wang JJ, Gaston LA, Zhou BY, Li ML, Xiao R, Wang Q, Zhang ZQ, Huang H, Liang W, Huang HT, Zhang XF (2018) An overview of carbothermal synthesis of metal-biochar composites for the removal of oxyanion contaminants from aqueous solution. Carbon J 129:674–687. https://doi.org/10.1016/j.carbon.2017.12.070

Li HC, Yu KW, Lien CH, Lin C, Yu CR, Vaidyanathan S (2023) Improving aquaculture water quality using dual-input fuzzy logic control for ammonia nitrogen management. J Mar Sci Eng 11(6):1109. https://doi.org/10.3390/jmse11061109

Liang PY, Yu HO, Huang JL, Zhang YT, Cao HY (2016) The review on adsorption and removing ammonia nitrogen with biochar on its mechanism. MATEC Web Conf J 67:1–11. https://doi.org/10.1051/matecconf/20166707006

Lingamdinne LP, Vemula KR, Chang YY, Yang JK, Karri RR, Koduru JR (2020) Process optimization and modeling of lead removal using iron oxide nanocomposites generated from bio-waste mass. Chemosphere J 243:125257. https://doi.org/10.1016/j.chemosphere.2019.125257

Liu Q, Liu BJ, Zhang YH, Hu TL, Lin ZB, Liu G, Wang XJ, Ma J, Wang H, Jin HY, Ambus P, Amonette JE, Xie ZB (2019) Biochar application as a tool to decrease soil nitrogen losses (NH3 volatilization, n2o emissions, and n leaching) from croplands: options and mitigation strength in a global perspective. Glob Change Biol 25(6):2077–2093. https://doi.org/10.1111/gcb.14613

Liu W, Chen SQ, Mei ZW, Li L, Li HF, Zhao WY, Tao H (2024a) Boron and nitrogen doping modulating the coordination environment of copper in biochar for reformative electrocatalytic CO_2 reduction. Surf Interfaces 44:103608. https://doi.org/10.1016/j.surfin.2023.103608

Liu XW, Liu XG, Gao SJ (2024b) The electrochemical mechanism of biochar for mediating the product ratio of $N_2O/(N_2O + N_2)$ in the denitrification process. Sci Total Environ 951:175566. https://doi.org/10.1016/j.scitotenv.2024.175566

Lu JK, Li Y, Wang B, Hou BY, Du GT, Si HY (2024) Analysis of the adsorption and fixation process of ammonium nitrogen in arable soil by biochar based on molecular dynamics simulation. Sci Total Environ 930:172815. https://doi.org/10.1016/j.scitotenv.2024.172815

Pariyar P, Kumari K, Jain MK, Jadhao PS (2020) Evaluation of change in biochar properties derived from different feedstock and pyrolysis temperature for environmental and agricultural application. Sci Total Environ J 713:136433. https://doi.org/10.1016/j.scitotenv.2019.136433

Qin Y, Wang HS, Li XR, Cheng JJ, Wu WX (2017) Improving methane yield from organic fraction of municipal solid waste (OFMSW) with magnetic rice-straw biochar. Bioresour Technol J 245(1):1058–1066. https://doi.org/10.1016/j.biortech.2017.09.047

Qiu YP, Cheng HY, Xu C, Sheng D (2008) Surface characteristics of crop-residue derived black carbon and lead (II) adsorption. Water Res J 42(3):567–574. https://doi.org/10.1016/j.watres.2007.07.051

Ragauskas AJ, Williams CK, Davison BH, Britovsek G, Cairney J, Eckert CA, Frederick WJ, Hallett JP, Leak DJ, Liotta CL, Mielenz JR, Murphy R, Templer

R, Tschaplinski T (2006) The path forward for biofuels and biomaterials. Sci J 311(5760):484–489. https://doi.org/10.1126/science.1114736
Rashid M, Hussain Q, Khan KS, Alwabel MI, Hayat R, Akmal M, Ijaz SS, Alvi S, Rehman OU (2021) Carbon-based slow-release fertilizers for efficient nutrient management: synthesis, applications, and future research needs. Soil Sci Plant Nutr J 21(2):1144–1169. https://doi.org/10.1007/s42729-021-00429-9
Raza S, Miao N, Wang PZ, Ju XT, Chen ZJ, Zhou JB, Kuzyakov Y (2020) Dramatic loss of inorganic carbon by nitrogen-induced soil acidification in chinese croplands. Glob Change Biol 26(6):3738–3751. https://doi.org/10.1111/gcb.15101
Shang G (2019) Effects of liquid hot water pretreatment and modified biochar on the anaerobic digestion of wheat straw. Northwest a&f Univ D 8:72
Shang X, Yang L, Ouyang D, Zhang B, Zhang WY, Gu MY, Li J, Chen MF, Huang LH, Qian LB (2020) Enhanced removal of 1,2,4-trichlorobenzene by modified biochar supported nanoscale zero-valent iron and palladium. Chemosphere 249:126518. https://doi.org/10.1016/j.chemosphere.2020.126518
Shi M, Wang ZF, Zheng Z (2013) Effect of Na^+ impregnated activated carbon on the adsorption of NH_4^+-N from aqueous solution. Environ Sci J 25(8):1501–1510. https://doi.org/10.1016/S1001-0742(8)60227-7
Skic K, Adamczuk A, Gryta A, Boguta P, Tóth T, Jozefaciuk G (2024) Surface areas and adsorption energies of biochars estimated from nitrogen and water vapour adsorption isotherms. Sci Rep 14(1):1–14. https://doi.org/10.1038/s41598-024-81030-9
Song HH, WangM J, Garg A, Lin S (2024) Exploring mechanism of five chemically treated biochars in adsorbing ammonium from wastewater: understanding role of physiochemical characteristics. Biomass Convers Biorefin 14(5):5847–5859. https://doi.org/10.1007/s13399-020-01135-9
Stefaniuk M, Oleszczuk P, Bartminski P (2016) Chemical and ecotoxicological evaluation of biochar produced from residues of biogas production. J Hazard Mater J 318(15):417–424. https://doi.org/10.1016/j.jhazmat.2016.06.013
Sumaraj XZX, Sarmah AK, Padhye LP (2020) Acidic surface functional groups control chemisorption of ammonium onto carbon materials in aqueous media. Sci Total Environ 698:134193. https://doi.org/10.1016/j.scitotenv.2019.134193
Sun Y, Zhang ZZ, Sun YM, Yang GX (2020) One-pot pyrolysis route to Fe-N-Doped carbon nanosheets with outstanding electrochemical performance as cathode materials for microbial fuel cell. Int J Agric Biol Eng J 13(6):207–214. https://doi.org/10.25165/j.ijabe.20201306.5765
Tan CM, Zhang XD, Liao C, Huang YB, Zheng JM, Chen H, He HZ (2023) Optimization of fishbone biochar preparation process based on adsorption performance. Sustain Chem Pharm 32:101015. https://doi.org/10.1016/j.scp.2023.101015
Teli S, Soni S, Teli P, Agarwal S (2024) Recent insights into modified biochars: a half-decade study. J Mater Sci 59(39):18357–18394. https://doi.org/10.1007/s10853-024-10272-9
Tripathy S, Sahu S, Patel RK, Panda RB, Kar PK (2021) Efficient removal of Cr (VI) by polyaniline modified biochar from date (Phoenix dactylifera) seed. Groundw Sustain Dev J 15:100653. https://doi.org/10.1016/J.GSD.2021.100653
Wang ZH, Guo HY, Shen F, Yang G, Zhang YZ, Zeng YM, Wang LL, Xiao H, Deng SH (2015) Biochar produced from oak sawdust by lanthanum (La)-involved pyrolysis for adsorption of ammonium (NH_4^+), nitrate (NO_3^-), and phosphate (PO_4^{3-}). Chemosphere J 119:646–653. https://doi.org/10.1016/j.chemosphere.2014.07.084
Wang ZC, Sun GF, Zhang LP, Zhou W, Sheng J, Ye XM, Olaniran AO, Kana EBG, Shao HB (2022) Aging characteristics and fate analysis of liquid digestate ammonium nitrogen disposal in farmland soil. Water 14(16):2487. https://doi.org/10.3390/w14162487
Wang MY, Wang GH, Qian LN, Yong XY, Wang YJ, An W, Jia HH, Zhou J (2023) Biochar production using biogas residue and their adsorption of ammonium nitrogen and chemical oxygen demand in wastewater. Biomass Convers Biorefin 13(5):3881–3892. https://doi.org/10.1007/s13399-021-01510-0
Wu ZB, Zhong H, Yuan XZ, Wang H, Wang L, Chen XH, Zeng GG, Wu Y (2014) Adsorptive removal of methylene blue by rhamnolipid-functionalized graphene oxide from wastewater. Water Res J 67:330–344. https://doi.org/10.1016/j.watres.2014.09.026
Yu Q, Xia D, Li H, Ke LT, Wang YP, Wang HT, Zheng YM, Li QB (2016) Effectiveness and mechanisms of ammonium adsorption on biochars derived from biogas residues. RSC Adv J 6:88373–88381. https://doi.org/10.1039/C6RA16913A
Zhang JZ, Ma XF, Yuan L, Zhou DX (2020) Comparison of adsorption behavior studies of Cd^{2+} by vermicompost biochar and $KMnO_4^-$ modified vermicompost biochar. J Environ Manage J 256:109959. https://doi.org/10.1016/j.jenvman.2019.109959
Zheng XB, Yang ZM, Xu XH, Shi XS, Dai M, Guo RB (2018a) Distillers' grains anaerobic digestion residue biochar used for ammonium sorption and its effect on ammonium leaching from an Ultisol. Environ Sci Pollut Res J 25:14563–14574. https://doi.org/10.1007/s11356-018-1681-3
Zheng XB, Yang ZM, Xu XH, Dai M, Guo RB (2018b) Characterization and ammonia adsorption of biochar prepared from distillers' grains anaerobic digestion residue with different pyrolysis temperatures. J Chem Technol Biotechnol J 93(1):198–206. https://doi.org/10.1002/jctb.5340
Zheng XB, Shi T, Song WJ, Xu L, Dong JX (2020) Biochar of distillers' grains anaerobic digestion residue: influence of pyrolysis conditions on its characteristics and ammonium adsorptive optimization. Waste Manag Res 38:86–97. https://doi.org/10.1177/0734242X19893021
Zheng XB, Dong JX, Zhang WH, Xiang J, Yin XS, Han LF (2021) Biogas residue biochar shifted bacterial community, mineralization, and molecular structure of organic carbon in a sandy loam Alfisol. GCB Bioenergy J 13:838–848. https://doi.org/10.1111/gcbb.12813
Zhu XJ, Ros GH, Xu MG, Xu DH, Cai ZJ, Sun N, Duan YG, Vries W (2024) The contribution of natural and anthropogenic causes to soil acidification rates under different fertilization practices and site conditions in southern China. Sci Total Environ 934:172986. https://doi.org/10.1016/j.scitotenv.2024.172986